Seyedi Hosseininia, E. (2013). *Géotechnique* **63**, No. 10, 830–841 [http://dx.doi.org/10.1680/geot.12.P.055]

Stress–force–fabric relationship for planar granular materials

E. SEYEDI HOSSEININIA*

This paper presents the theoretical development of a relationship between the average stress components and the micromechanical fabric anisotropy characteristics within assemblies of planar particles. The main feature of the modified formulation is the ability to consider both inherent and induced anisotropy conditions within the assembly. This was achieved by amending the definition of the contact vector between particles in the stress–force–fabric relationship. By using numerical discrete-element method (DEM), a series of inherently anisotropic granular materials were simulated in order to verify the accuracy of the proposed formulation. In the simulations, the geometry of the particles was chosen to be irregular polygons. The shear capacity of the assemblies during the loading process was calculated from direct measurement of macroscopic stress components, and from anisotropy fabric parameters. By comparing the results, it is shown that reasonable agreement exists between the calculated and measured values.

KEYWORDS: anisotropy; constitutive relations; numerical modelling; shear strength; stress analysis

INTRODUCTION

It is clear that an understanding of the mechanical behaviour of granular media is highly dependent upon comprehension of the micromechanical response of these systems. To interpret the mechanical behaviour of granular materials, the fabric should be studied: that is, the spatial arrangement of soil particles, contact points and associated voids. Finding a relationship between applied forces or stresses exerted on boundaries and fabric evolution within the assembly is an interesting subject in this regard.

Experimental investigations on the behaviour of a granular material go back to Schneebeli (1956), who worked on an assembly of metal rods. Further attempts to model granular materials were made using optically sensitive materials (Dantu, 1957; Wakabayashi, 1957; Drescher & de Josselin de Jong, 1972; Oda & Konishi, 1974, Oda *et al.*, 1982). In this method, an assembly of photoelastic cylindrical rods was loaded through platens, and the interparticle contact forces were calculated from the pattern of isochromatics viewed in polarised light. Based on the experimental results, granular media were studied from analytical points of view.

Biarez & Wiendieck (1963) presented the distribution of contacts in graphical form as rosettes (i.e. histograms) for two-dimensional assemblies of irregularly shaped particles. Then, based on statistical functions, the distribution of contacts was introduced for assemblies including uniform spheres (Horne, 1965) and non-spherical particles (Oda, 1972a, 1972b, 1972c, 1977; Rothenburg, 1980). Satake (1982) described the distribution of contact normals for planar systems of particles by a second-order anisotropy tensor, and Oda *et al.* (1982) and Mehrabadi *et al.* (1982) proposed a three-dimensional tensorial quantity called the fabric tensor.

Regarding the estimation of stress state for a granular assembly, Hill (1963) defined the average stress tensor in terms of applied forces over a homogeneous granular system (see also Drescher & de Josselin de Jong, 1972; Strack & Cundall, 1978; Rothenburg, 1980; Mehrabadi *et al.*, 1982). Weber (1966) introduced a macroscopic stress tensor, which can be calculated from assembly contact forces and the geometrical arrangement of contacting particles. This relationship became the origin of most micromechanical investigations of granular assemblies.

Based on Weber's equation, Rothenburg (1980) showed that the average stress tensor for an assembly comprising circular particles or spheres has the properties of the stress tensor as used in continuum mechanics, but is derived from consideration of discrete contact forces, contact geometry and principles of static equilibrium. He assumed that contact forces and contact vectors are homogeneously distributed among a very large number of particles, and thus he approximated the distribution of discrete contact force components and contact normals of particles by statistical continuous functions. He developed useful relationships for assemblies with planar particles (discs), which equate the micromechanical parameters to the macro-scale shear capacity of the system. By assuming that the distributions of average contact force components and contact normals have the same directions of anisotropy, the so-called stress–force–fabric relationship is introduced as (Rothenburg & Selvadurai, 1981)

$$\frac{\sigma_t}{\sigma_n} = \frac{a_c + a_n + a_t}{2 + a_c a_n} \tag{1}$$

where σ_t and σ_n are the deviatoric and normal stress-invariant quantities respectively. The ratio σ_t/σ_n is frequently interpreted as the mobilised angle of friction for cohesionless materials (i.e. $\sin\phi_{mob}$). This equation directly relates the shear capacity of the assembly to the anisotropy development in terms of coefficients of anisotropy for normal contacts (a_c), average normal contact force (a_n), and tangential contact force (a_t).

In order to verify the stress–force–fabric equation quantitatively, detailed information is needed for the distribution of contact normals and contact force components among a large number of particles. Since experimental tests cannot easily give the required information, numerical simulations of granular media by the discrete-element method (DEM) were used for verification. The accuracy of the stress–force–fabric relationship was verified for assemblies including circular discs (Rothenburg & Bathurst, 1989) and planar

Manuscript received 26 April 2012; revised manuscript accepted 24 October 2012. Published online ahead of print 8 March 2013.
Discussion on this paper closes on 1 January 2014, for further details see p. ii.
* Department of Civil Engineering, Faculty of Engineering, Ferdowsi University of Mashhad, Iran.

elliptical particles (Rothenburg & Bathurst, 1992). The elongated elliptical particles were homogeneously distributed within the assembly. Later, it was shown that the aforementioned macro–micro relationship was also applicable to convex polygon-shaped particles (Mirghasemi *et al.*, 2002). Note that the particles used in these simulations were randomly distributed within the assembly, or the shapes of particles were equilateral polygons – that is, having isotropic shapes (Mirghasemi *et al.*, 2002). Later, Seyedi Hosseininia & Mirghasemi (2006) verified the so-called stress–force–fabric relationship for assemblies comprising breakable, polygon-shaped particles. Since the geometry of both intact and broken particles was chosen to be isotropic rather than elongated, equivalence between the macro and micro parts of equation (1) was still satisfied. All the studies mentioned above with non-circular particles imply that the stress–force–fabric relationship is applicable if the fabric of assemblies (particle orientation) has an isotropic condition, rather than being directionally anisotropic.

When elongated particles are used, it is evident that the fabric anisotropy is highly dependent upon the alignment and spatial arrangement of particles. Practically all soil structures, whether natural or man made, are influenced by a gravitational field that induces an anisotropic condition in the soil fabric. During the deposition process of soil particles – similar to what happens in river, beach or coastal dune sands, or in artificially deposited sand layers – particles tend to be aligned in a preferred direction, and hence an initial inherent anisotropy is generated in the soil fabric.

There have been many experimental attempts (Arthur & Menzies, 1972; Oda *et al.*, 1978, 1985; Ishibashi *et al.*, 1991; Lade *et al.*, 2008) as well as analytical and numerical studies (Ting & Meachum, 1995; Azami *et al.*, 2010; Chang & Yin, 2010; Mahmood & Iwashita, 2010; Sazzad & Suzuki, 2010; Fu & Dafalias, 2011) to investigate the effect of inherent anisotropy on the macroscopic mechanical properties of inherently anisotropic materials. As mentioned above, the DEM is a powerful tool that makes it possible to investigate micromechanical features of granular materials.

Using the DEM, several studies have focused on the evolution of microstructure – that is, the magnitude and direction of fabric anisotropy of inherently anisotropic assemblies. For instance, Nouguier-Lehon *et al.* (2003) studied the influence of grain shape and angularity on the behaviour of granular materials. By following the value of local variables related to fabric and particle orientation, they found in particular that the coincidence of the principal axes of the fabric tensor with those of the stress tensor exists for discs and isotropic particles from the very beginning of the loading. By contrast, this process initiates very gradually for elongated particles that are inclined horizontally or vertically.

Peña *et al.* (2009) reported the results of numerical biaxial compression tests on isotropic and elongated angular particles (with vertical and horizontal arrangements) from a micromechanical point of view. They showed that the major direction of the stress tensor is the same for both particle shapes, irrespective of the initial orientation. This comes from the direction of force chains carrying the largest stresses along the loading axis. Furthermore, based on the results of their simulations, they concluded that for isotropic particles the contact orientation is governed by the direction of the major component of the stress tensor, and for elongated particles mainly by the major principal direction of the inertia tensor, which is related to the particle orientation.

Fu & Dafalias (2011) investigated the fabric evolution within shear bands of granular materials using elliptical particles in the DEM. They concluded that the angle between the mean particle orientation and the mean contact-normal orientation should be dependent on a number of internal variables of the assembly, such as the interparticle friction angle, particle shape and particle size.

Mahmood & Iwashita (2010) simulated a series of biaxial compression tests using the DEM with different bedding planes of elliptical particles. They again confirmed that the bedding angle (initial anisotropy) influences the evolution of contact anisotropy; the principal mean direction of contact normals is not coincident with the direction of the loading axis. Rather, the initial value is equal to the bedding direction, and it varies depending on the bedding plane during the loading process. It was also found that the mean direction of fabric anisotropy inside shear bands tends to be rotated towards the loading axis at large shear deformation.

More recently, Seyedi Hosseininia (2012b) examined fabric evolution within inherently anisotropic granular assemblies containing angular particles by DEM simulations. He observed the same qualitative trends as found in the references mentioned above. He showed that variation of the direction of fabric anisotropy depends on the initial direction of the particle bedding plane, whereas the major mean direction of normal and tangential contact forces rotates suddenly towards the loading axis, irrespective of the initial bedding plane condition.

Based on the discussion above, it is clear that the proposed stress–force–fabric relationship (equation (1)) does not hold true for inherently anisotropic assemblies, since the anisotropy directions of the force components are not coincident with that of the fabric – that is, particle orientation. The present paper investigates the accuracy of the stress–force–fabric relationship for inherently anisotropic granular materials, and proposes a new form of the expression. First, the theoretical background is briefly reviewed, and then required modifications to the equation are explained. The proposed relationship will be verified by performing numerical simulations of several biaxial compression tests using the DEM with different bedding planes of elongated angular particles.

THEORETICAL BACKGROUND

Interparticle load transfer between particles can be described by a contact force vector $\boldsymbol{f}$ applied to the contact point. The study of the microstructure (fabric) can be performed by introducing a contact normal $\boldsymbol{n}$, denoting the unit vector orthogonal to the contact tangent plane, and a contact vector $\boldsymbol{l}$ describing the line pointing from the mass centre of the contacting particle to the contact point (Rothenburg, 1980). Fig. 1 shows the definitions of the contact normal, contact vector and force vector for two contacting particles. Conditions of static equilibrium in a granular assembly lead to the expression for the Cauchy stress tensor related to using microscopic averages, which describes the geometry and force distributions in a granular assembly as (Rothenburg & Selvadurai, 1981)

$$\sigma_{ij} = m_{\mathrm{v}} \int_0^{2\pi} \bar{f}_i(\theta)\bar{l}_j(\theta)E(\theta)\mathrm{d}\theta \quad i,j = 1,2 \tag{2}$$

where the term m_{v} is the density of contacts (the number of contacts per unit area), and $E(\theta)$ is the normalised contact orientation distribution defining the relative frequency of contacts with orientation θ. Assuming that θ is the inclination with respect to the horizontal direction (1–1 axis), the contact orientation can be defined by the contact-normal components as $\boldsymbol{n} = (\cos\theta, \sin\theta)$. $\bar{f}_i(\theta)$ and $\bar{l}_j(\theta)$ represent the polar distributions of the average components of the force vector and contact vector respectively.

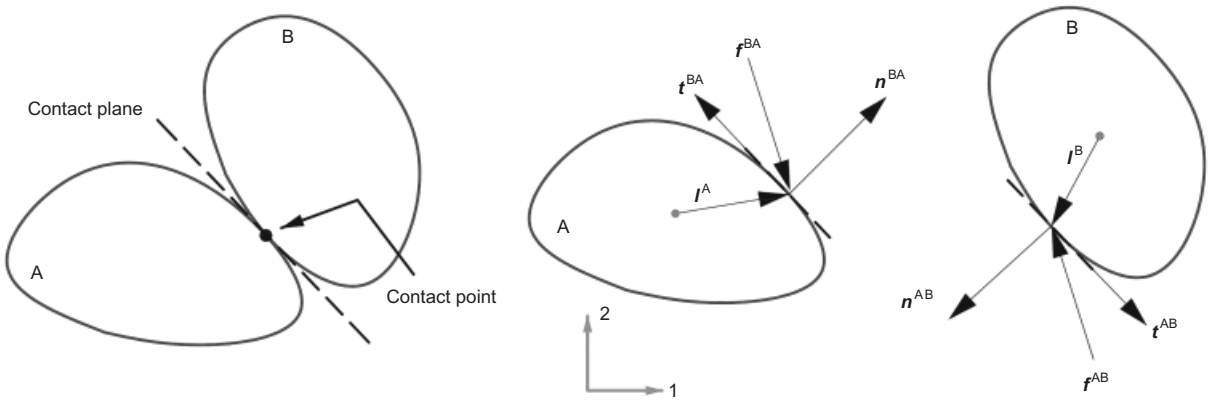

Fig. 1. Schematic diagrams of two contacting particles and associated contact vector (*l*), force vector (*f*), normal contact vector (*n*) and tangential contact vector (*t*)

The average contact force acting on contacts with orientation θ can be decomposed into an average normal force component $\bar{f}_{\mathrm{n}}(\theta)$ and an average tangential force component $\bar{f}_{\mathrm{t}}(\theta)$. Therefore

$$\bar{f}_i(\theta) = \bar{f}_{\mathrm{n}}(\theta)n_i + \bar{f}_{\mathrm{t}}(\theta)t_i \tag{3}$$

For a granular assembly comprising circular particles, the contact vector is coaxial with the contact normal: that is, $\boldsymbol{l} = \bar{l}_0\boldsymbol{n}$. Here $\bar{l}_0$ is the average length of the contact vector, and is approximately equal to the average radius. In equation (3), $\boldsymbol{t} = (-\sin\theta, \cos\theta)$ represents the direction orthogonal to $\boldsymbol{n}$, according to Fig. 1. Hence, by substituting equation (3) in equation (2), it can be simplified to

$$\sigma_{ij} = m_{\mathrm{v}}\bar{l}_0 \int_0^{2\pi} \left[\bar{f}_{\mathrm{n}}(\theta)n_i(\theta) + \bar{f}_{\mathrm{t}}(\theta)t_i(\theta)\right]E(\theta)\mathrm{d}\theta \qquad i, j = 1, 2 \tag{4}$$

If the distribution of fabric quantities (i.e. the frequency of contacts, E, the average normal contact force, $\bar{f}_{\mathrm{n}}$, and the average tangential contact force, $\bar{f}_{\mathrm{t}}$) is sketched in a polar system, the polar distribution forms a peanut-like histogram, such as that shown in Fig. 2(a). Based on the measured histogram data, the polar distribution can be estimated by introducing functions in terms of the coefficient of anisotropy, a_i, and the major principal direction of anisotropy, θ_i. According to Fig. 2(b), the parameter θ_i indicates the angle between the long axis of the histogram with respect to the horizontal direction, and a_i describes the circularity degree of the histogram. The parameter a_i is defined as $(A_1 - A_2)/(A_1 + A_2)$, in which A_1 is the length of the axis of the histogram along the major principal direction, and A_2 is the length along the perpendicular direction. Thus the value of a_i varies from 0 to 1. If the histogram has the form of a circle, the value of a_i is 0, which corresponds to an isotropic distribution. However, the value of a_i increases and closes to 1 if the circle deforms as a peanut, which indicates a high degree of anisotropy. The procedure to obtain the anisotropy parameters based on the histogram data is explained in Seyedi Hosseininia (2012b).

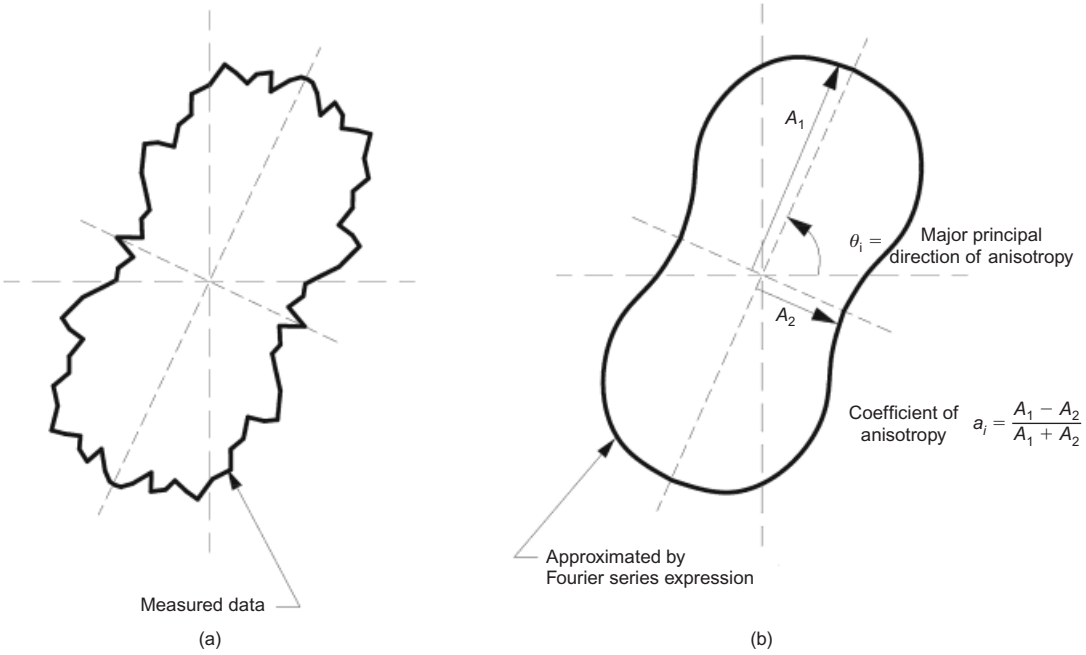

Fig. 2. Polar distribution of a fabric quantity: (a) based on measured data; (b) estimated by a Fourier series expression

Polar distributions of average contact force components and contact-normal distribution can be approximated by second-order Fourier series expressions as follows (Rothenburg, 1980).

$$E(\theta) = \frac{1}{2\pi}[1 + a_c \cos 2(\theta - \theta_c)] \tag{5a}$$

$$\bar{f}_n(\theta) = \bar{f}_0[1 + a_n \cos 2(\theta - \theta_n)] \tag{5b}$$

$$\bar{f}_t(\theta) = \bar{f}_0[a_w - a_t \sin 2(\theta - \theta_t)] \tag{5c}$$

where a_c describes the anisotropy in contact orientations, and θ_c is the major principal direction of anisotropy. $\bar{f}_0$ is a constant representing the average normal force over all contacts in the assembly. The terms a_n, a_t and a_w are non-dimensional coefficients of contact force anisotropy. Similar to θ_c, the terms θ_n and θ_t represent preferred directions of contact force distributions for normal and tangential components respectively. For a general loading path, θ_n is not equal to θ_t, but they have almost the same value under monotonic loading. In contrast to a_c and a_n, the term a_w is not independent, and can be defined in terms of a_c and a_t from moment equilibrium of all contacts. Generally, the value of a_w is small, and close to zero. Physically, a non-zero value corresponds to a situation in which a non-symmetrical distribution of shear contact forces is required to compensate for the lack of contact normals in the direction of loading axis. Such a condition may occur in inherently anisotropic granular assemblies. In the Appendix, the derivation of a general expression for the parameter a_w in terms of the other anisotropy parameters is explained, and the formulation is verified, based on the measured data.

The anisotropy parameters mentioned above can be also determined by introducing second-order symmetric fabric tensors (including contact frequency and contact forces). The coefficients of anisotropy are related to the second invariant of the deviatoric part of the corresponding fabric tensor, and the corresponding direction of anisotropy represents the major principal direction (or eigenvector) of these tensors (Bathurst & Rothenburg, 1992).

According to the Mohr stress circle, the invariants of the average stress tensor have the forms

$$\sigma_n = \frac{\sigma_{11} + \sigma_{22}}{2} \tag{6a}$$

$$\sigma_t = \sqrt{\left(\frac{\sigma_{11} - \sigma_{22}}{2}\right)^2 + \sigma_{12}^2} \tag{6b}$$

The ratio of the above two invariants is generally known as the mobilised friction angle for cohesionless granular materials. By putting the Fourier series expressions in equation (5) into the integral of equation (4), the stress tensor components can be obtained. Finally, after some mathematical manipulation, and ignoring the product of anisotropy coefficients for the third and higher orders, the stress invariants can be calculated, and their ratio takes the form

$$\frac{\sigma_t}{\sigma_n} = \frac{\sqrt{a_c^2 + a_n^2 + a_t^2 + 2a_c a_n \cos 2(\theta_c - \theta_n) + 2a_c a_t \cos 2(\theta_c - \theta_t) + 2a_n a_t \cos 2(\theta_n - \theta_t)}}{2 + a_c a_n \cos 2(\theta_c - \theta_n)} \tag{7}$$

The above equation is the origin of the so-called stress–force–fabric relationship, which links the macroscopic mobilised stress to the microscopic anisotropy parameters within the assembly. If the directions of anisotropy for contact normals and contact forces are coaxial – that is, $\theta_c = \theta_n = \theta_t$ – then the simplified expression indicated as equation (1) is obtained. As explained in the Introduction section, the coaxiality between fabric anisotropy and force anisotropy exists only for assemblies containing circular particles or isotropic (near-circular) particles. This situation holds true for elongated particles only if the particles are homogeneously distributed within the assembly. Hence it is clear that the relationship should be modified for inherently anisotropic assemblies, where the distribution of contacts is no longer isotropic.

DEVELOPMENTS

A relationship between the average stress tensor and the fabric characteristics was obtained for granular assemblies containing circular particles (equation (7)). The main reason for success in formulating such a relationship is that, owing to the geometry of the particles, it is possible to define the contact vector in terms of the contact normal. This implies that the fabric anisotropy takes effect only from the anisotropy of contact-normal distribution. However, this does not hold true for elongated particles. In the simplest form, consider three pairs of contacting particles with circular and elliptical shapes, as shown in Fig. 3(a). The contact normals in all groups of contacting particles have the same direction. It is clear that, for circular particles, no difference exists if the particles are inclined towards the other direction. For elliptical particles, however, it can be seen that although the directions of contact normals in the two groups are identical, the particle inclinations are different from each other. This indicates that fabric anisotropy is also related to the distribution of particle orientations. This matter has been already given attention in the literature (e.g. Oda, 1993; Nüebel & Rothenburg, 1996; Peña *et al.*, 2009). However, it is not appropriate to consider solely the orientation of particles as a parameter in describing the fabric anisotropy. As shown in Fig. 3(b), consider three pairs of contacting particles. Although the relative inclination (β) of particles is identical in all groups, the directions of the contact normal in each group are different from each other.

The explanations above imply that the relationship $\boldsymbol{l} = \bar{l}_0 \boldsymbol{n}$ is not satisfied for elongated particles because of non-coincidence of the contact vector with the contact normal, and also the variability of the contact length ($\bar{l}_0$) due to the particle geometry. The latter reason becomes more pronounced for an assemblage of elongated particles with the same bedding planes.

In order to address this deficiency, it is suggested that the contact vector be introduced with respect to the contact plane rather than only the contact normal. In other words, the contact vector is decomposed into normal and orthogonal components with respect to the corresponding contact plane. In such conditions, the normal and tangential components of the contact vector can implicitly reflect the effect of particle orientation. As a consequence, the average contact vector acting on contacts with orientation θ can be decomposed into an average normal contact component $\bar{l}_n(\theta)$ and an average tangential contact component $\bar{l}_t(\theta)$. Therefore

$$\bar{l}_i(\theta) = \bar{l}_n(\theta) n_i + \bar{l}_t(\theta) t_i \tag{8}$$

Applying this decomposition to equation (2), obtains

$$\sigma_{ij} = m_v \int_0^{2\pi} \begin{bmatrix} \bar{f}_n(\theta)\bar{l}_n(\theta) n_i n_j + \bar{f}_n(\theta)\bar{l}_t(\theta) n_i t_j \\ + \bar{f}_t(\theta)\bar{l}_n(\theta) t_i n_j + \bar{f}_t(\theta)\bar{l}_t(\theta) t_i t_j \end{bmatrix} E(\theta) \mathrm{d}\theta \tag{9}$$

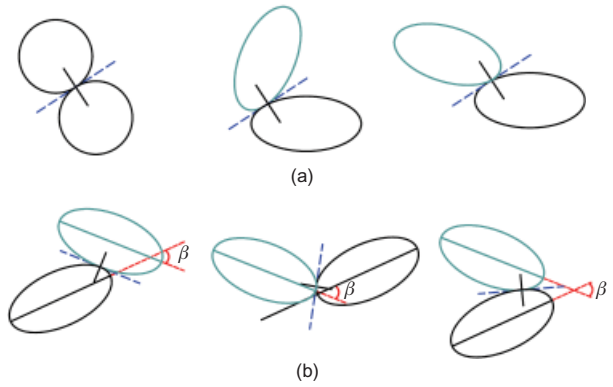

Fig. 3. (a) Contacting particles with the same contact normal but different orientations; (b) contacting particles with the same orientation but different contact normals

Similar to what Rothenburg suggested for the distribution of average contact force components, the following Fourier series expressions are suggested for the average normal and tangential contact components.

$$\bar{l}_{\mathrm{n}}(\theta) = \bar{l}_0[1 + a_{\mathrm{ln}} \cos 2(\theta - \theta_{\mathrm{ln}})] \tag{10a}$$

$$\bar{l}_{\mathrm{t}}(\theta) = -\bar{l}_0 a_{\mathrm{lt}} \sin 2(\theta - \theta_{\mathrm{lt}}) \tag{10b}$$

The term $\bar{l}_0$ in the above equations represents the average normal component of contact vectors from all particles in the assembly. The terms a_{ln} and a_{lt} are non-dimensional coefficients of contact anisotropy. The coefficient a_{ln} explains the anisotropic distribution of the normal component of the contact vectors within the assembly. Therefore a non-zero value can be obtained even for a packing of circular particles. A non-zero value for the coefficient a_{lt} represents the deviation of the direction of the contact vector from the contact normal. Hence, for a packing of circular particles, a_{lt} becomes zero. Nevertheless, the reverse conclusion may not be correct. It means that in an assembly of elongated particles it is possible to have $a_{\mathrm{lt}} \approx 0$, which means that the elongated particles are homogeneously distributed within the assembly. The terms θ_{ln} and θ_{lt} represent certain preferred directions of particles contact. For a general case, where the assembly contains a broad range of sizes of irregularly shaped particles with a random distribution, $\theta_{\mathrm{ln}} \neq \theta_{\mathrm{lt}}$, but for assemblies containing similar particles, these directions are nearly coincident. For instance, the value of these terms for inherently anisotropic assemblies with the same particle shape is nearly equal to the bedding angle of the particles.

An approach similar to that introduced by Rothenburg (1980) for the determination of anisotropic parameters is taken into consideration in order to define the quantities a_{ln}, a_{lt}, θ_{ln} and θ_{lt}. The coefficient terms and directions of anisotropy are related to the invariant quantities and the principal directions (eigenvectors) of new fabric tensors respectively. Two symmetric second-order fabric tensors LN_{ij} and LT_{ij} can be defined from discrete numerical simulation data using the approximations

$$LN_{ij} = \frac{1}{2\pi}\int_0^{2\pi} \bar{l}_{\mathrm{n}}(\theta) n_i n_j \mathrm{d}\theta \approx \frac{1}{N_{\mathrm{g}}} \sum_{\theta_{\mathrm{g}}} \bar{l}^{\mathrm{c}}_{\mathrm{n}} n^{\mathrm{c}}_i n^{\mathrm{c}}_j$$

$$LT_{ij} = \frac{1}{2\pi}\int_0^{2\pi} \bar{l}_{\mathrm{t}}(\theta) t_i n_j \mathrm{d}\theta \approx \frac{1}{N_{\mathrm{g}}} \sum_{\theta_{\mathrm{g}}} \bar{l}^{\mathrm{c}}_{\mathrm{t}} t^{\mathrm{c}}_i n^{\mathrm{c}}_j \tag{11}$$

where N_{g} is the number of orientation intervals used in the approximation, and θ_{g} is the average orientation of the particle group. The tensor LN_{ij} indicates the anisotropy in the distribution of average normal contact components, and similarly the tensor LT_{ij} corresponds to the distribution of average tangential contact components. Hence the above-mentioned anisotropy parameters are defined by

$$a_{\mathrm{ln}} = \frac{2\sqrt{(LN_{11} - LN_{22})^2 + 4LN_{12}^2}}{LN_{11} + LN_{22}}, \quad \tan 2\theta_{\mathrm{ln}} = \frac{2LN_{12}}{LN_{11} - LN_{22}} \tag{12a}$$

$$a_{\mathrm{lt}} = \frac{2\sqrt{(LT_{11} - LT_{22})^2 + 4LT_{12}^2}}{LT_{11} + LT_{22}}, \quad \tan 2\theta_{\mathrm{lt}} = \frac{2LT_{12}}{LT_{11} - LT_{22}} \tag{12b}$$

Returning to equation (9), the components of the average stress tensor can now be obtained explicitly in terms of anisotropic parameters. By performing mathematical manipulations, the calculation of the stress invariants based on the stress tensor components leads to the expressions

$$\sigma_{\mathrm{n}} = \frac{m_{\mathrm{v}} \bar{l}_0 \bar{f}_0}{2} \times \left[\begin{array}{l} 1 + \frac{1}{2} a_{\mathrm{c}} a_{\mathrm{n}} \cos 2(\theta_{\mathrm{c}} - \theta_{\mathrm{n}}) + \frac{1}{2} a_{\mathrm{c}} a_{\mathrm{ln}} \cos 2(\theta_{\mathrm{c}} - \theta_{\mathrm{ln}}) \\ + \frac{1}{2} a_{\mathrm{n}} a_{\mathrm{ln}} \cos 2(\theta_{\mathrm{n}} - \theta_{\mathrm{ln}}) + \frac{1}{2} a_{\mathrm{t}} a_{\mathrm{lt}} \cos 2(\theta_{\mathrm{t}} - \theta_{\mathrm{lt}}) \end{array} \right] \tag{13a}$$

$$\sigma_{\mathrm{t}} = \frac{m_{\mathrm{v}} \bar{l}_0 \bar{f}_0}{4} \times \left[\begin{array}{l} a_{\mathrm{c}}^2 + a_{\mathrm{n}}^2 + a_{\mathrm{t}}^2 + a_{\mathrm{ln}}^2 + a_{\mathrm{lt}}^2 + 2a_{\mathrm{c}} a_{\mathrm{n}} \cos 2(\theta_{\mathrm{c}} - \theta_{\mathrm{n}}) \\ + 2a_{\mathrm{c}} a_{\mathrm{t}} \cos 2(\theta_{\mathrm{c}} - \theta_{\mathrm{t}}) + 2a_{\mathrm{c}} a_{\mathrm{ln}} \cos 2(\theta_{\mathrm{c}} - \theta_{\mathrm{ln}}) \\ + 2a_{\mathrm{c}} a_{\mathrm{lt}} \cos 2(\theta_{\mathrm{c}} - \theta_{\mathrm{lt}}) + 2a_{\mathrm{n}} a_{\mathrm{t}} \cos 2(\theta_{\mathrm{n}} - \theta_{\mathrm{t}}) \\ + 2a_{\mathrm{n}} a_{\mathrm{ln}} \cos 2(\theta_{\mathrm{n}} - \theta_{\mathrm{ln}}) + 2a_{\mathrm{n}} a_{\mathrm{lt}} \cos 2(\theta_{\mathrm{n}} - \theta_{\mathrm{lt}}) \\ + 2a_{\mathrm{t}} a_{\mathrm{ln}} \cos 2(\theta_{\mathrm{t}} - \theta_{\mathrm{ln}}) + 2a_{\mathrm{t}} a_{\mathrm{lt}} \cos 2(\theta_{\mathrm{t}} - \theta_{\mathrm{lt}}) \\ + 2a_{\mathrm{ln}} a_{\mathrm{lt}} \cos 2(\theta_{\mathrm{ln}} - \theta_{\mathrm{lt}}) \end{array} \right]^{1/2} \tag{13b}$$

As a consequence, the shear capacity of an assembly with arbitrary particle shapes and inherent anisotropy can be obtained from microscopic anisotropy coefficients from the stress-invariant ratio mentioned in equation (6). If an assembly of circular particles is considered under monotonic loading, the geometry of particles implies that $a_{\mathrm{lt}} = 0$. Owing to the monotonic nature of the loading, $\theta_{\mathrm{c}} = \theta_{\mathrm{n}} = \theta_{\mathrm{t}} = \theta_{\mathrm{ln}}$. Moreover, if the particles have a narrow range of diameters, a_{ln} would have a small value close to zero. Hence the same relationship as expressed in equation (1) can be obtained by simplifying the fabric conditions of granular materials.

The same approach mentioned above can be also applied to three-dimensional systems. The stress–force–fabric relationship for two-dimensional systems is expressed by Fourier series expansions (equation (13)) in terms of trigonometric functions. For three-dimensional systems, however, the equations would be extremely cumbersome, and a tensorial Fourier series expansion should be used (e.g. Thornton & Barnes, 1986).

VERIFICATION OF THE PROPOSED FORMULATION

Numerical simulations

In order to examine the stress–force–fabric relationship developed here (equations (13a) and (13b)), a series of biaxial compression tests were simulated, using the DEM. The key point in the simulations is that the particles are not circular or elliptical in shape, but have a geometry of a convex, irregular polygon. Schematic diagrams of the particle geometry and dimensions used in the simulations are depicted in Fig. 4. The particles were intentionally considered to be elongated along the horizontal direction (long axis of particles). In the process of sample generation, three sizes of these particles were used with scale ratios of 0·75, 1·0 and 1·25 with respect to those presented in Fig. 4. The gradation of such an aggregate is characterised by a uniformity coefficient (D_{60}/D_{10}) of 1·35 and a curvature coefficient ($D_{30}^2/D_{10}D_{60}$) 1·2. Here D_x indicates the long axis length (diameter of an equivalent circumscribed circle) of soil particles for which x% of the particles are finer. In total, five series of samples were generated. The samples have the form of a circle with diameter 160 mm. About 2000 particles exist in each sample. Having the same frequency distribution of particles, these samples were distinguished by the initial inclination of the particles before shearing. In one assembly, the particles were inclined randomly, which constitutes an isotropic-like fabric. However, the other four assemblies contained particles whose elongation was inclined along a predefined direction, that is, $\alpha = 0°$, 30°, 60° and 90°, where α is the bedding angle, which is defined by the angle between the long axis of the particle and the horizontal direction (1–1 axis). As a consequence, the latter four samples were inherently anisotropic.

After generation of the samples, each assembly was compressed to a confining pressure of 300 kPa ($= \sigma_{11} = \sigma_{22}$). The compression process was continued until there was almost no volume change in the assembly. Fig. 5(a) represents a quarter of the compacted assemblies for all inherently anisotropic samples under the confining pressure of 300 kPa. As shown, the average inclination of all particles in each sample was oriented towards the defined bedding angle (α). The compacted assembly was then sheared biaxially. This loading was performed by keeping the lateral stress (σ_{11}) equal to 300 kPa while the boundary was simultaneously forced to move along the 2–2 axis by a constant vertical displacement rate. Thus the sample was deformed to be an ellipse, elongated horizontally. The biaxially sheared samples with different bedding angles are depicted in Fig. 5(b). The numerical procedure and the dataset used in this work are the same as those mentioned by Seyedi Hosseininia (2012a, 2012b), and detailed descriptions of the various stages of the simulations can be found in those papers.

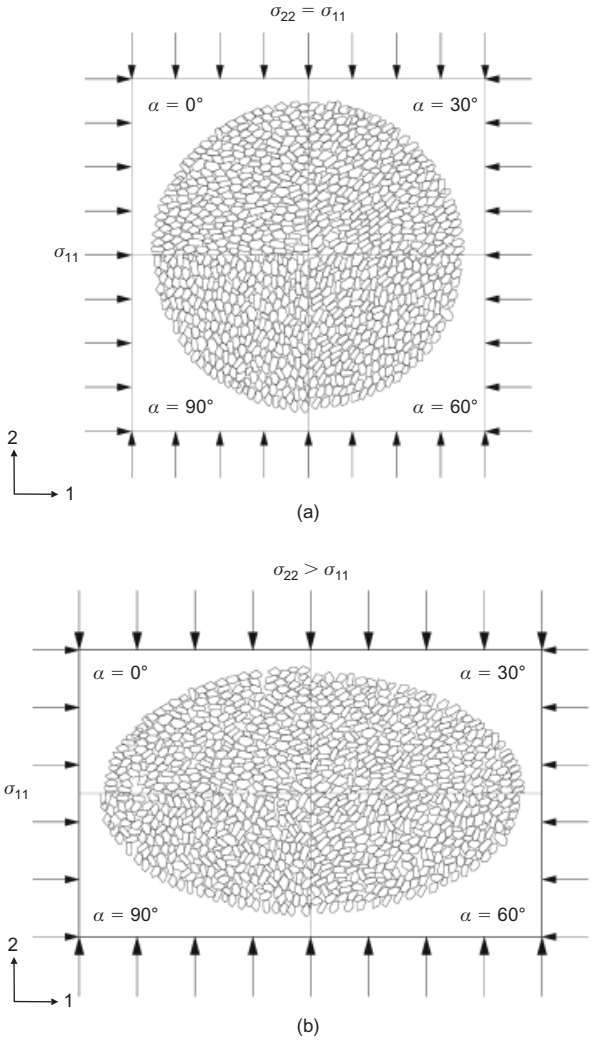

Fig. 5. Schematic diagrams of one quarter of: (a) isotropically compacted assemblies; (b) biaxially sheared assemblies under lateral constant pressure at axial strain of 20%

Evolution of anisotropy parameters in fabric

The general idea of how the microstructure in granular assemblies evolves during the shearing process may be usefully studied by following the change in the number of contacts. Fig. 6 shows the variation of the normal contact anisotropy coefficient (a_c) and the corresponding principal direction of anisotropy (θ_c) against the axial strain for isotropic and all inherently anisotropic assemblies. According to Fig. 6(a), the initial value of the parameter a_c, which corresponds to the end of the compaction process, is the same for all inherently anisotropic samples. Such equality in a_c originates from the identical state of isotropic compaction

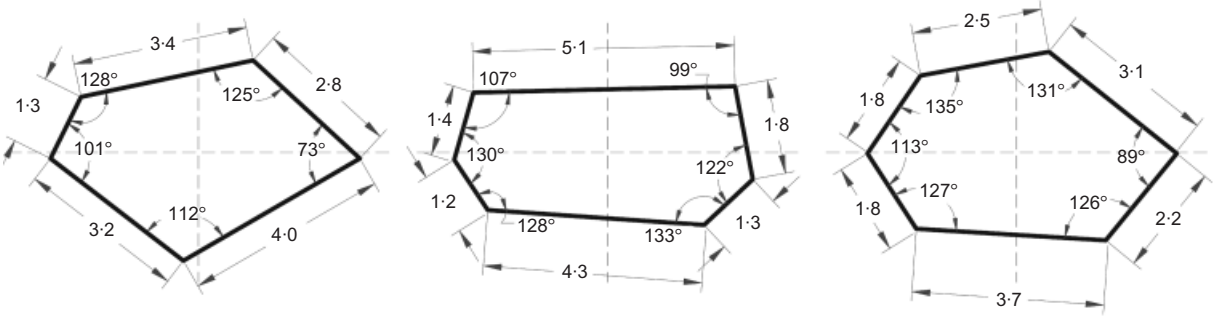

Fig. 4. Geometry of particles used in simulations (dimensions in mm)

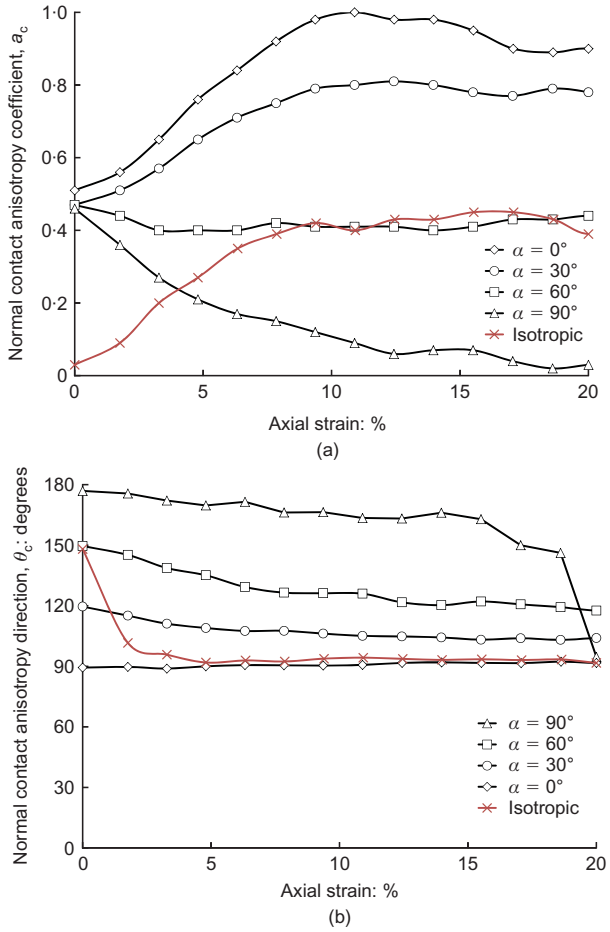

Fig. 6. Evolution of normal contact anisotropy parameters

of all assemblies, regardless of the bedding angle. However, the subsequent variation of the contact anisotropy depends on the arrangement and bedding angle of particles. The assemblies with $\alpha = 0°$ and 30° show a growth in a_c such that it reaches the limiting value of 1 with $\alpha = 0$, whereas it remains at around its initial value in the sample with $\alpha = 60°$. In the assembly with $\alpha = 90°$, contacts tend to be distributed isotropically, as the loading continues after a_c starts to decrease from the onset of loading, and it reaches close to zero at large axial strains ($\varepsilon_{22} = 20\%$). Considering the isotropic sample, as expected, a_c starts from a small value close to zero. As the loading process continues, it reaches a limiting value (= 0·5), similar to what happened for $\alpha = 60°$. It then remains constant until the end of loading. The growth in a_c indicates that new contacts are generated among particles along the principal direction of anisotropy, and simultaneously contacts are lost along the perpendicular direction. The reverse phenomenon causes a reduction in a_c.

The variation of the major principal direction of contact anisotropy (θ_c) is depicted in Fig. 6(b) as a function of axial strain. As a global trend, one can observe that, in inherently anisotropic assemblies, the direction of anisotropy initially coincides with the perpendicular direction of the bedding angle – that is, $\theta_c \approx 90° + \alpha$. However, θ_c gradually tends to rotate towards the loading axis ($\theta_c = 90°$). In the isotropic assembly, however, the trend is different, and there is a rapid rotation of the anisotropy direction towards the loading axis at small axial strain level. For a small value of a_c, such as exists at the beginning of loading for an isotropic assembly, and at large deformation for $\alpha = 90°$, the direction of anisotropy does not make sense, since it has an isotropic distribution.

The variation of the normal contact force anisotropy coefficient (a_n) as a function of axial strain is plotted in Fig. 7(a) for all assemblies. The influence of inherent anisotropy on the increase of a_n can be easily found in the graphs. First, the mobilised value of a_n increases with decrease of the bedding angle. Second, the peak value of a_n occurs at larger axial strains as the bedding angle decreases. For the isotropic sample, after reaching the peak value at a small strain level, the parameter a_n gains a value similar to that of the sample with $\alpha = 60°$. Fig. 7(b) depicts the principal direction of normal contact force anisotropy. Before loading starts, the anisotropy direction is inclined approximately perpendicular to the bedding angle, but it rotates rapidly towards the loading axis ($\theta_n \approx 90°$) in all assemblies. Such a rotation of anisotropy axis originates from the generation of new force chains along the loading axis, irrespective of the arrangement of particles, and in turn, the magnitude of the force chains along the tensile (horizontal) direction is disintegrated. A graphical evolution of force chains during the loading process is presented by Seyedi Hosseininia (2012b).

According to Fig. 8(a), the coefficient of tangential contact force anisotropy, a_t, shows a rapid rise to a maximum value, which is followed by a very slow reduction in magnitude at large axial strain. The variation of a_t for isotropic and anisotropic samples is almost the same. The initial increase in a_t corresponds to the development of frictional resistance as a result of the relative movement of particles. The magnitude of a_t is much less than that of a_c and a_n because of the limiting interparticle resistance, which leads to particle slippage. The variation in the principal orientation of the tangential contact forces, θ_t, is depicted in Fig. 8(b). Analogous to what happens for the normal contact force, θ_t rotates abruptly at the initial stage of loading

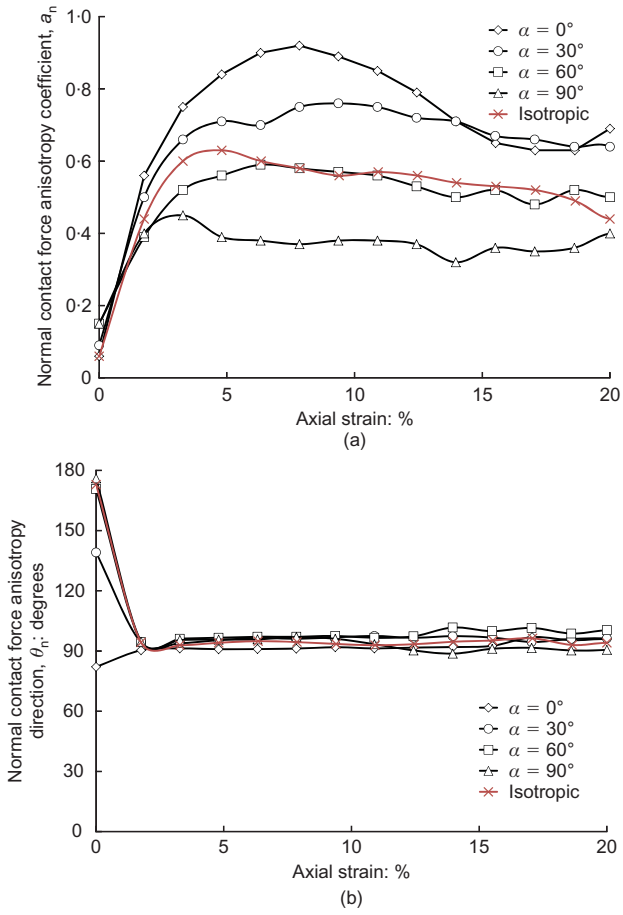

Fig. 7. Evolution of normal contact force anisotropy parameters

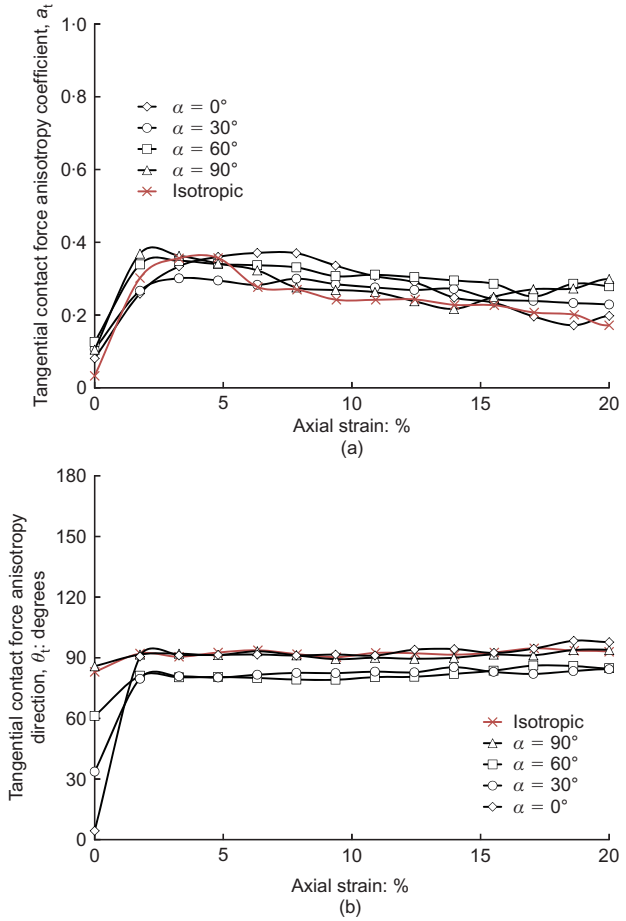

Fig. 8. Evolution of tangential contact force anisotropy parameters

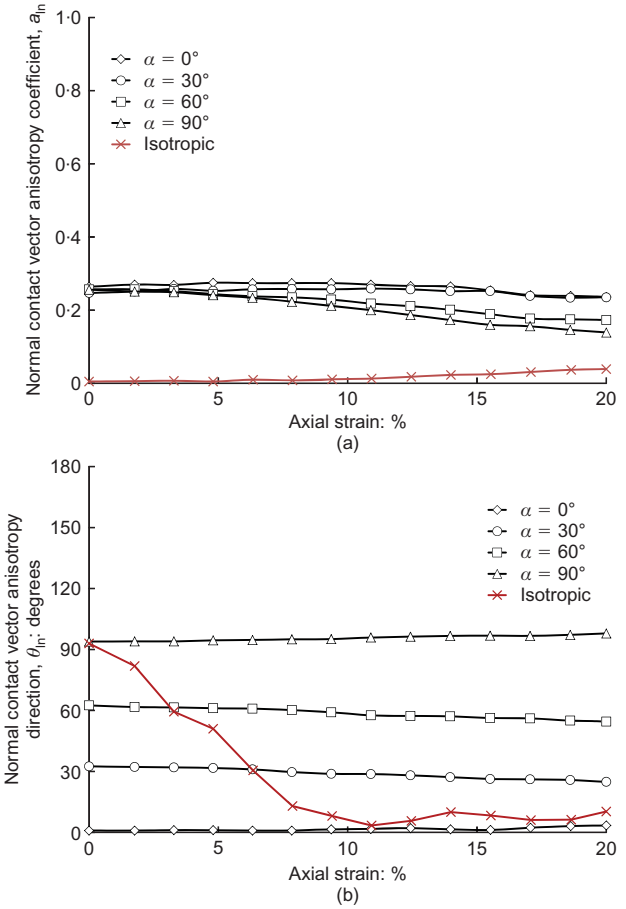

Fig. 9. Evolution of normal contact vector anisotropy parameters

towards the loading axis; there is a small diversion of about 10° for the samples with $\alpha = 30°$ and 60°.

The same strategy can be applied to tracking the variation of anisotropy of contact-length components. Figs 9 and 10 present the variation of anisotropy parameters against the shear deformation for normal contact (a_{ln}, θ_{ln}) and tangential contact (a_{lt}, θ_{lt}) components respectively. It can be seen that since the particles are randomly distributed in the isotropic sample, both a_{ln} and a_{lt} are almost zero during the whole of the loading process. However, the inherently anisotropic samples contain contact-length anisotropy from the beginning, and after a small rise in magnitude, they both tend to decrease slowly as the shear deformation continues. It is important to note that the anisotropy coefficient of the tangential contact length component is not zero and its magnitude is greater than that of the normal component. This proves that the assumption of coaxiality between the contact vector and the contact normal, which can exist among circular particles or in isotropic samples, is not in general correct. Although the variation trend in a_{ln} and a_{lt} is almost the same for all anisotropic samples, it is interesting to note that the rate of decrease in contact-length anisotropy for the samples with $\alpha = 60°$ and 90° is much higher than that of the others. Such a reduction in a_{ln}, a_{lt} indicates that the particles tend to rotate, and that the particles are inclined

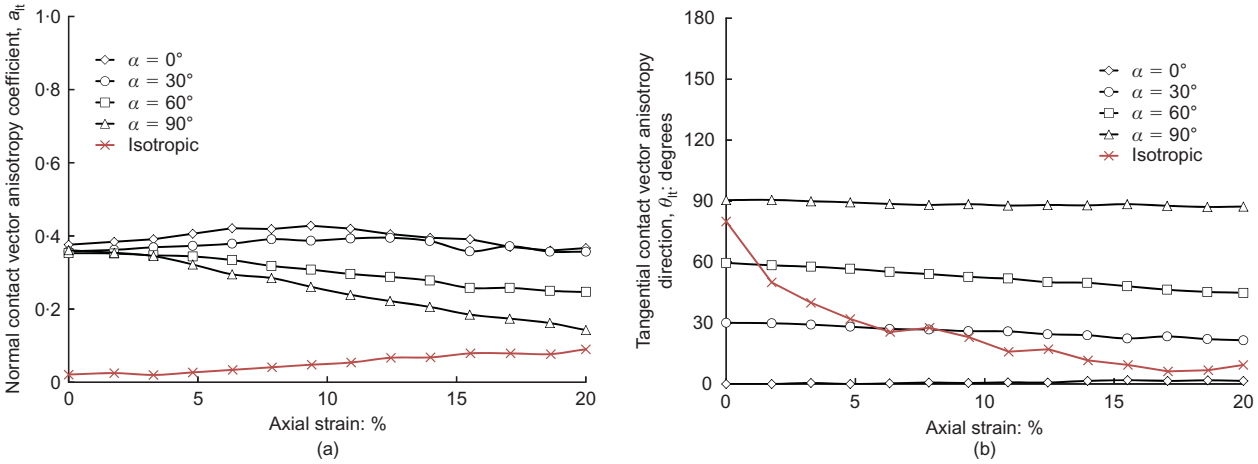

Fig. 10. Evolution of tangential contact vector anisotropy parameters

in such a way that they can carry applied loads. A detailed comparison of the degree of particle rotation among anisotropic assemblies is given by Seyedi Hosseininia (2012a). Particle rotation occurs because of local instability of column-like structures, as explained elsewhere (Seyedi Hosseininia, 2012b). According to Figs 9(b) and 10(b), the principal direction of contact-length anisotropy of both normal and tangential components remains almost constant in each sample, and is equal to the bedding angle. This is due to the elongation of particles, which is oriented towards their bedding angle. Since the anisotropy coefficient of the isotropic sample is close to zero, the rotation of anisotropy direction shown in Figs 9(b) and 10(b) is not meaningful.

Measured and microscopically predicted values of shear resistance

As well as tracing the anisotropy parameters during the biaxial compression test, the stress components (i.e. σ_{11}, σ_{22}, σ_{12}) of the assemblies were measured during the loading process. As a consequence, it is possible to calculate the variation of the stress-invariant ratio σ_t/σ_n directly from equation (6). On the other hand, the stress-invariant ratio can be calculated from a micromechanical point of view by substituting the values of the parameters a_c, a_n, a_t, a_{ln}, a_{lt}, θ_c, θ_n, θ_t, θ_{ln} and θ_{lt} into equation (13), which is developed for a general condition. The results are sketched in Fig. 11 in terms of stress-invariant ratio against axial strain for both isotropic and anisotropic samples ($\alpha = 0°$, 30°, 60° and 90°). As can be seen, the stress–force–fabric expression is in good agreement with the measured data.

In order to investigate the accuracy of the previous versions of the stress–force–fabric expression, they are also calculated, based on the required anisotropy parameters, and the results are presented in the corresponding figures. A comparison between the isotropic (and hence coaxial) form of the stress–force–fabric relationship (equation (1)) and that based on measurement shows that the accuracy of the equation depends on the bedding angle as well as on the axial strain level. It overestimates the shear resistance of the granular assembly for the whole range of axial strain level with bedding angles of $\alpha = 0°$, 30° and 60°, whereas for the assembly with $\alpha = 90°$, the obtained stress ratio is higher for a small range of deformation and lower than the measured value after the peak point. However, this relationship can predict the measured stress ratio for the isotropic sample, as expected. The other form of the stress–force–fabric equation, which considers the non-coaxiality of anisotropy

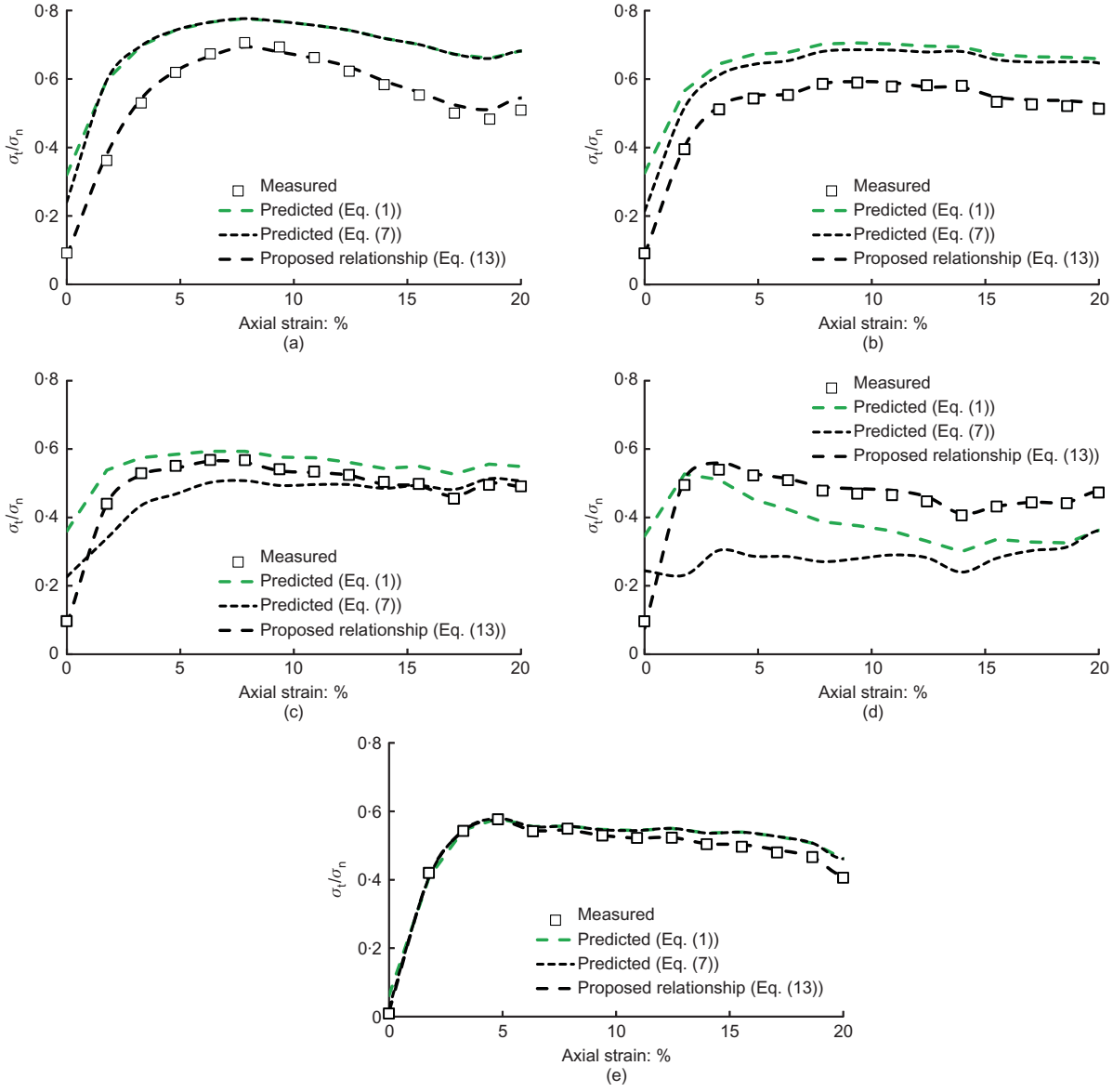

Fig. 11. Comparison of stress-invariant ratio values between measurements and predictions by anisotropy parameters: (a) $\alpha = 0°$; (b) $\alpha = 30°$; (c) $\alpha = 60°$; (d) $\alpha = 90°$; (e) randomly distributed particles

parameters (equation (7)), is also calculated, as shown in Fig. 11. A comparison between the results indicates that this form of the relationship does not predict the stress ratio with any accuracy, and the prediction becomes worse as the bedding angle increases. Obviously it gives a good prediction of the stress ratio for the isotropic sample. It is important to note that in both the latter forms of the expressions, it is assumed that the contact vector is coaxial with the contact normal. Such a comparison between the results clearly expresses the importance of consideration of non-coaxiality between the contact vector and the contact normal.

CONCLUSIONS

In this paper, a stress–force–fabric expression is developed for a general condition of planar, granular materials. This equation presents a relationship between fabric anisotropy parameters and the macroscopic stress state of the assembly. The proposed expression is based on consideration of the normal and tangential components of the contact vector with respect to the contact plane of two adjacent contacting particles. The proposed equation can predict the stress state of inherently anisotropic assemblies in which the particles are irregularly shaped, and are directionally oriented with respect to the loading axis. The numerical results have shown that the contact vector is not coaxial with the contact normal, in general. As a consequence, the so-called stress–force–fabric relationship already used for circular particles or homogeneous samples is not able to predict a correct value of the stress state for a general condition.

ACKNOWLEDGEMENTS

The author would like to express his appreciations to the Research Deputy of Ferdowsi University of Mashhad for supporting the present research by grant no. 20563-25/11/90. The author would also like to thank Dr Ali Lashkari from Shiraz University of Technology for his valuable comments on this manuscript.

APPENDIX: DERIVATION OF THE PARAMETER a_w

Referring to equation (5c), the term a_w can be assessed as follows.

$$a_w = \frac{\bar{f}_t(\theta)}{\bar{f}_0} + a_t \sin 2(\theta - \theta_t) \tag{14}$$

By integrating the above equation over the range 0–2π, the following is obtained

$$a_w = \frac{1}{2\pi \bar{f}_0} \int_0^{2\pi} \bar{f}_t(\theta) \mathrm{d}\theta \tag{15}$$

On the other hand, with the same integration of equation (5b), the average normal contact force ($\bar{f}_0$) can be calculated as

$$\bar{f}_0 = \frac{1}{2\pi} \int_0^{2\pi} \bar{f}_n(\theta) \mathrm{d}\theta \tag{16}$$

By combining equations (15) and (16), and applying the summation rules for the integrals, a_w can be approximated as

$$a_w = \frac{\int_0^{2\pi} \bar{f}_t(\theta) \mathrm{d}\theta}{\int_0^{2\pi} \bar{f}_n(\theta) \mathrm{d}\theta} \approx \frac{\sum_{i=1}^{N_c} f_s^i}{\sum_{i=1}^{N_c} f_n^i} \tag{17}$$

where N_c indicates the total number of contacts within the assembly. As a result, a_w can be measured directly from the summation of the tangential and normal contact forces.

From a micromechanical point of view, as already mentioned, a_w can be defined in terms of other anisotropy parameters. A stationary particulate material is in static equilibrium. Moment equilibrium of interparticle forces for the whole of such a particulate system requires that

$$\int_0^{2\pi} [\bar{f}_n(\theta)\bar{l}_t(\theta) - \bar{f}_t(\theta)\bar{l}_n(\theta)] E(\theta) \mathrm{d}\theta = 0 \tag{18}$$

The above equality can be also deduced from the definition of the Cauchy stress tensor, in which it is necessary to have $\sigma_{ij} = \sigma_{ji}$, $i \neq j$. By substituting the corresponding Fourier series expressions into equation (18), a general expression for a_w can be assessed, after some mathematical manipulations, to give

$$a_w = -\frac{\begin{array}{l} a_c a_t \sin 2(\theta_c - \theta_t) + a_c a_{lt} \sin 2(\theta_c - \theta_{lt}) \\ + a_n a_{lt} \sin 2(\theta_n - \theta_{lt}) + a_t a_{ln} \sin 2(\theta_t - \theta_{ln}) \end{array}}{2 + a_c a_{ln}[1 + \cos 2(\theta_c - \theta_{ln})]} \tag{19}$$

In order to verify the above equation, the measured values of the anisotropy parameters a_c, a_n, a_t, a_{lt}, θ_c, θ_n, θ_t, θ_{ln} and θ_{lt} are substituted, and the results are compared with the directly measured values of a_w. Fig. 12 shows the variation of measured and predicted values of a_w for the isotropic and all inherently anisotropic assemblies. As shown, there is a good agreement between the results, which validates the obtained formulation. The term a_w has a small value, which fluctuates around zero for the samples with $\alpha = 0°$ and 90°, as well as the isotropic one, whereas it reaches about 0·25 for the other two anisotropic samples ($\alpha = 30°$, 60°). As explained earlier, a non-zero value of a_w corresponds to a non-symmetrical distribution of shear contact forces, which originates from the non-coincidence of contact force anisotropy and contact anisotropy.

NOTATION

a_c coefficient of contact-normal anisotropy
a_{ln} coefficient of contact-normal vector anisotropy
a_{lt} coefficient of contact-tangential vector anisotropy

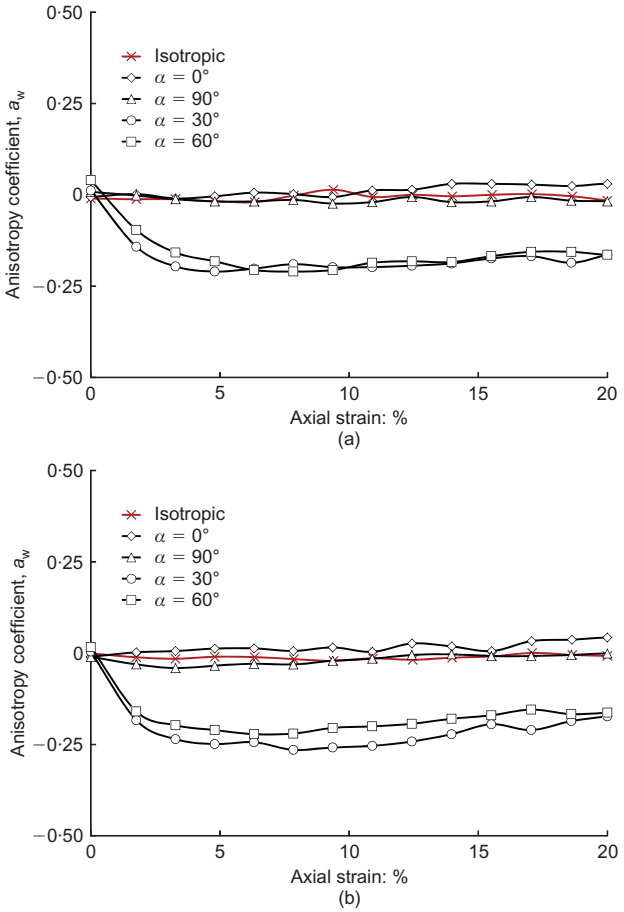

Fig. 12. Comparison of anisotropy coefficient a_w during shear deformation: (a) measured; (b) predicted

a_n	coefficient of contact-normal force anisotropy
a_t, a_w	coefficients of contact-tangential force anisotropy
$E(\theta)$	contact-normal distribution function
$\boldsymbol{f}$	force vector
$\bar{f}_0$	average normal contact force
$\bar{f}_n(\theta)$, $\bar{f}_t(\theta)$	distribution of average normal and tangential contact forces
LN_{ij}	symmetric second-order tensor for normal contact vector
LT_{ij}	symmetric second-order tensor for tangential contact vector
$\bar{l}_n(\theta)$, $\bar{l}_t(\theta)$	distribution of average normal and tangential contact vectors
$\bar{l}_0$	average length of contact vector
m_v	number of contacts per volume (contact density)
$\boldsymbol{n}$	normal contact vector
$\boldsymbol{t}$	tangential contact vector
α	bedding angle of particles
θ	inclination with respect to the horizontal direction (1–1 axis)
θ_c	major principal direction of contact anisotropy
θ_{ln}	major principal direction of contact-normal vector anisotropy
θ_{lt}	major principal direction of contact-tangential vector anisotropy
θ_n	major principal direction of contact-normal force anisotropy
θ_t	major principal direction of contact-tangential force anisotropy
σ_{ij}	stress tensor
σ_n, σ_t	normal and deviatoric stress invariants of stress tensor
ϕ_{mob}	mobilised friction angle

REFERENCES

Arthur, J. R. F. & Menzies, B. K. (1972). Inherent anisotropy in a sand. *Géotechnique* **22**, No. 1, 115–128, http://dx.doi.org/10.1680/geot.1972.22.1.115.

Azami, A., Pietruszczak, S. & Guo, P. (2010). Bearing capacity of shallow foundations in transversely isotropic granular media. *Int. J. Numer. Analyt. Methods Geomech*. **34**, No. 8, 771–793.

Bathurst, R. J. & Rothenburg, L. (1992). Investigation of micromechanical features of idealized granular assemblies using DEM. *Engng Comput*. **9**, No. 2, 199–210.

Biarez, J. & Wiendieck, K. (1963). La comparaison qualitative entre l'anisotropie mécanique et l'anisotropie de structure des milieux pulvérulents. *C. R. Acad. Sci*. **256**, 1217–1220 (in French).

Chang, C. S. & Yin, Z.-Y. (2010). Micromechanical modeling for inherent anisotropy in granular materials. *J. Geotech. Engng* **136**, No. 7, 830–839.

Dantu, P. (1957). Contribution à l'étude mécanique et géométrique des milieux pulvérulents. *Proc. 4th Int. Conf. Soil Mech. Geotech. Engng, London* **1**, 144–148 (in French).

Drescher, A. & de Josselin de Jong, G. (1972). Photoelastic verification of a mechanical model for the flow of a granular material. *J. Mech. Phys. Solids* **20**, No. 5, 337–351.

Fu, P. & Dafalias, Y. F. (2011). Study of anisotropic shear strength of granular materials using DEM simulation. *Int. J. Numer. Analyt. Methods Geomech*. **35**, No. 10, 1098–1126.

Hill, R. (1963). Elastic properties of reinforced solids: some theoretical principles. *J. Mech. Phys. Solids* **11**, No. 6, 357–372.

Horne, M. R. (1965). The behavior of an assembly of rotund, rigid, cohesionless particles. I and II. *Proc. R. Soc. London Ser. A* **286**, 62–97.

Ishibashi, I., Chen, Y.-C. & Chen, M.-T. (1991). Anisotropic behavior of Ottawa sand in comparison with glass spheres. *Soils Found*. **31**, No. 1, 145–155.

Lade, P. V., Nam, J. & Hong, W.P. (2008). Shear banding sand cross-anisotropic behavior observed in laboratory sand tests with stress rotation. *Can. Geotech. J.* **45**, No. 1, 74–84.

Mahmood, Z. & Iwashita, K. (2010). Influence of inherent anisotropy on mechanical behavior of granular materials based on DEM simulations. *Int. J. Numer. Analyt. Methods Geomech*. **34**, No. 8, 795–819.

Mehrabadi, M. M., Nemat-Naser, S. & Oda, M. (1982). On statistical description of stress and fabric in granular materials. *Int. J. Numer. Analyt. Methods Geomech*. **6**, No. 1, 95–108.

Mirghasemi, A. A., Rothenburg, L. & Matyas, E. L. (2002). Influence of particle shape on engineering properties of assemblies of two-dimensional polygon-shaped particles. *Géotechnique* **52**, No. 3, 209–217, http://dx.doi.org/10.1680/geot.2002.52.3.209.

Nouguier-Lehon, C., Cambou, B. & Vincens, E. (2003). Influence of particle shape and angularity on the behaviour of granular materials: a numerical analysis. *Int. J. Numer. Analyt. Methods Geomech*. **27**, No. 14, 1207–1226.

Nüebel, K. & Rothenburg, L. (1996). Particle shape effect in stress–force–fabric relationship for granular media. *J. Mech. Behav. Mater*. **7**, No. 3, 219–233.

Oda, M. (1972a). Deformation mechanism of sand in triaxial compression tests. *Soils Found*. **12**, No. 4, 45–63.

Oda, M. (1972b). Initial fabrics and their relations to mechanical properties of granular material. *Soils Found*. **12**, No. 1, 18–36.

Oda, M. (1972c). The mechanism of fabric changes during compressional deformation of sand. *Soils Found*. **12**, No. 2, 1–18.

Oda, M. (1977). Co-ordination number and its relation to shear strength of granular material. *Soils Found*. **17**, No. 2, 29–42.

Oda, M. (1993). Inherent and induced anisotropy in plasticity theory of granular soils. *Mech. Mater*. **16**, No. 1–2, 35–45.

Oda, M. & Konishi, J. (1974). Rotation of principal stresses in granular material during simple shear. *Soils Found*. **14**, No. 4, 39–53.

Oda, M., Koishikawa, I. & Higuchi, T. (1978). Experimental study of anisotropic shear strength of sand by plane strain test. *Soils Found*. **18**, No. 1, 26–38.

Oda, M., Konishi, J. & Nemat-Nasser, S. (1982). Experimental micromechanical evolution of strength of granular materials: effects of particle rolling. *Mech. Mater*. **1**, No. 4, 269–283.

Oda, M., Nemat-Naser, S. & Konishi, J. (1985). Stress-induced anisotropy in granular masses. *Soils Found*. **25**, No. 3, 85–97.

Peña, A. A., McNamara, S., Lind, P. G. & Herrmann, H. J. (2009). Avalanches in anisotropic sheared granular media. *Granular Matter* **11**, No. 4, 243–252.

Rothenburg, L. (1980). *Micromechanics of idealized granular systems*. PhD thesis, Department of Civil Engineering, Carlton University, Ottawa, Canada.

Rothenburg, L. & Bathurst, R. J. (1989). Analytical study of induced anisotropy in idealized granular materials. *Géotechnique* **39**, No. 4, 601–614, http://dx.doi.org/10.1680/geot.1989.39.4.601.

Rothenburg, L. & Bathurst, R. J. (1992). Micromechanical features of granular assemblies with planar elliptical particles. *Géotechnique* **42**, No. 1, 79–95, http://dx.doi.org/10.1680/geot.1992.42.1.79.

Rothenburg, L. & Selvadurai, A. P. S. (1981). A micromechanical definition of the Cauchy stress tensor for particulate media. In *Mechanics of structured media* (ed. A. P. S. Selvadurai), pp. 469–486. Amsterdam, the Netherlands: Elsevier.

Satake, M. (1982). Fabric tensor in granular materials. In *Proceedings of the IUTAM symposium on deformation and failure of granular materials* (eds P. A. Vermeer and H. J. Luger), pp. 63–68. Rotterdam, the Netherlands: Balkema.

Sazzad, M. M. & Suzuki, K. (2010). Micromechanical behavior of granular materials with inherent anisotropy under cyclic loading using 2D DEM. *Granular Matter* **12**, No. 6, 597–605.

Schneebeli, G. (1956). Une mécanique pour les terres sans cohésion. *C. R. Acad. Sci*. **243**, 2647–2673 (in French).

Seyedi Hosseininia, E. (2012a). Discrete element modeling of inherently anisotropic granular assemblies with polygonal particles. *Particuology* **10**, No. 5, 542–552.

Seyedi Hosseininia, E. (2012b). Investigating the micromechanical evolutions within inherently anisotropic granular materials using discrete element method. *Granular Matter* **14**, No. 4, 483–503.

Seyedi Hosseininia, E. & Mirghasemi, A. A. (2006). Numerical simulation of breakage of two-dimensional polygon-shaped particles using discrete element method. *Powder Technol*. **166**, No. 2, 100–112.

Strack, O. D. L. & Cundall, P. A. (1978). *The distinct element method as a tool for research in granular media: Report to the National Science Foundation concerning NSF Grant ENG75-*

20711. National Science Foundation, Department of Civil and Mining Engineering, University of Minnesota, Minneapolis and St. Paul, MN, USA.

Thornton, C. & Barnes, D. J. (1986). Computer simulated deformation of compact granular assemblies. *Acta Mech*. **64**, No. 1–2, 45–61.

Ting, J. M. & Meachum, L. R. (1995). Effect of bedding plane orientation on the behavior of granular systems. In *Mechanics of materials with discontinuities and heterogeneities* (eds A. Misra and C. S. Chang), pp. 43–57. New York, NY, USA: ASME.

Wakabayashi, T. (1957). Photoelastic method for determination of stress in powdered mass. *Proc. 7th Japanese Nat. Cong. on Applied Mechanics, Tokyo*, 153–158.

Weber, J. (1966). Recherches concernant les contraintes intergranulaires dans les milieux pulvérulents. *Bull. Liaison Ponts et Chaussées* **20**, Juillet–Août, 3-1–3-20.